2-E-5

GFP reporter を用いたマウス骨折治癒過程における woven bone 形成の評価

牛久 智加良[1]　Douglas J. Adams[2]
David W. Rowe[3]　斎藤 充[1]　丸毛 啓史[1]

【目的】われわれはこれまでに，ラット1型コラーゲン(Col 3.6)およびヒトオステオカルシン(hOC)プロモーター領域を使い，骨芽細胞の分化段階に応じてGFP(Green fluorescence protein)が発現するDual Transgenic(Tg)マウスを作製し，石灰化過程における細胞分化と基質合成の関係について報告してきた．今回，骨折治癒における仮骨の石灰化過程について同モデルを用いて解析したので報告する．

【方法】Col3.6GFPcyan, hOCGFPtpz dual Tgマウス(8週齢)の脛骨に閉鎖式骨折を作製した．骨折後7，10，14と30日目に脛骨を回収し蛍光顕微鏡を用いてGFPの発現を観察した．また屠殺前にXylenol orange(XO)を投与し，石灰化評価とHEおよびSafranin O染色による組織学的評価も行った．

【結果】骨折後7日目になると，仮骨部にCol3.6陽性細胞(Col3.6+)に囲まれたXO陽性の膜性骨化によるwoven bone(w/b)を認めた．10日目には，その表面に多くのCol 3.6-hOC両陽性細胞が観察され，w/bはその厚みを増していた．14日目までに軟骨は内軟骨性骨化によるw/bに置換された．この時，仮骨中心部のw/bは主にCol3.6+に囲まれていたのに対し，骨折部，new cortical shellでは主にCol3.6-hOC両陽性細胞に囲まれていた．30日目には，仮骨中心部のw/bは骨髄様組織に置換されたが，骨折部，new cortical shellではその厚みを増していた．

【考察】これまで仮骨石灰化過程は，w/b形成を放射線，組織学的に観察することで評価されてきた．しかしその過程をGFP dual Tgマウスを用いて観察すると，hOC陽性細胞に囲まれたw/bが仮骨部に残存するのに対し，Col3.6陽性細胞に囲まれたw/bは早期に骨髄様組織に置換されることが明らかとなった．GFPトランスジェニックマウスを用いた骨折モデルでは，分化度の異なる細胞が仮骨石灰化過程に及ぼす影響を時間的に空間的に解析することが可能である．今後，骨折治癒過程に及ぼす薬剤や力学刺激などの影響を評価するモデルとして有用と考えられる．

[1]慈恵医大整形　[2]Dept. of Orthop. Surg., School of Medicine, Univ. of Connecticut Health Center, Farmington, CT, USA
[3]Dept. of Reconstructive Sciences, School of Dental Medicine, Univ. of Connecticut Health Center, Farmington, CT, USA

2-E-6

低出力超音波パルス治療の骨癒合リモデリング期に対する効果　—マイクロCTを用いた仮骨の髄腔化・皮質骨化の定量評価—

飛田 健治　大西 五三男　松本 卓也　大橋 暁
別所 雅彦　松山 順太郎　金子 雅子　中村 耕三

【背景】低出力超音波パルス(以下LIPUS)治療の骨癒合への促進効果は臨床・基礎研究から実証されている．マイクロCT(以下μCT)は硬組織試料の非侵襲的三次元形態評価ができ，骨折治癒過程の精確な評価が可能である．骨折のリモデリング期は仮骨の皮質骨化と共に髄腔化が起こり，骨癒合強度の回復に非常に重要であるが，これらをμCTを用いて三次元的に定量評価した先行研究はない．

【目的】LIPUS照射がリモデリング期の仮骨に及ぼす効果をμCTを用いて評価する．

【材料と方法】21-23週齢，体重約4 kgで雄の日本白色家兎を用いた．吸入麻酔下右脛骨の骨切りを行い，2 mmのgapを作成し両側式の創外固定を行った．LIPUSの照射/非照射群に分け，観察期間を4および8週とした．LIPUS照射は，術後3日より1週間に6日，吸入麻酔下に20分間行い，非照射群は照射群と同様の条件でダミーの振動子を用いて模擬照射を行った．観察終了後と殺し，仮骨のμCT撮データを，骨量ファントムで定量化し評価した．対象部位はgapの中心1 mmとし200 mg/cm^{3}で2値化した仮骨をendosteal(以下E)，intercortical (I)，periosteal region (P)の3領域に分け，各領域におけるbone volume(以下BV)，bone mineral content(以下BMC)，BMC/BVの計測と，三次元的な二次モーメント，慣性モーメントとStress-Strain Index(以下SSI)から骨癒合強度予測を行った．LIPUS照射/非照射群の差の検定にはt検定を行った(有意水準<0.05)．

【結果】4週ではすべての評価項目で有意差が見られなかったが，8週において，LIPUS照射群は非照射群に対してBMC/BVはE，I，P共に有意に高値，BMCはEでは低下しており，I，Pで有意に高値，BVはIで有意に高値であった．また8週では二次モーメント，慣性モーメント，SSI共に有意に高値であった．

【考察】μCTを用いて，リモデリング期の仮骨髄腔化・皮質骨化に着目し定量評価した先行研究はない．今回の結果からLIPUSは仮骨の髄腔化・皮質骨化を促進した．またモーメント，SSIの増加からLIPUSは骨強度をより増加させることが示唆された．

東大大学院整形

Evaluation of Bone Strength Using Quantitative Computed Tomography Based Finite Element Method
- Clinical Application for the Diagnosis of Osteoporosis -

The Dept. of Orthopaedic Surgery, The University of Tokyo
Isao Ohnishi, Masahiko Bessho, Takuya Matsumoto, Masako Kaneko, Satoru Ohashi, Kazuhiro Imai, and Kozo Nakamura

The Computational Diagnostic Radiology and Preventive Medicine, The 22nd Century Medical Center, The University of Tokyo
Naoto Hayashi

The Dept. of Orthopaedic Surgery, Tokyo Metropolitan Geriatric Hospital
Fumiaki Tokimura

Tokyo Metropolitan Institute of Gerontology
Kim Hunkyung

Abstract

Fragility fractures are the most serious complication of osteoporosis and have been recognized as a major public health problem. It is essential to precisely quantify the strength of the fragile bone in order to estimate the fracture risk and plan preventive interventions. Quantitative computed tomography (QCT)-based finite element (FE) method (QCT/FEM) could possibly achieve precise assessment of the strength of the bone of interest. The purpose of the study was to create a simulation model that could accurately predict the strength and to apply this method in the wide range of clinical diagnosis in osteoporosis. We verified the accuracy of our model by load testing using fresh frozen cadaver specimens. The yield loads, fracture loads and principal strains of the prediction significantly correlated with those measured by load testing ($r=0.941$, 0.979, 0.963). FE analysis showed that the solid elements and shell elements in undergoing compressive failure were at the same region as the experimental fracture site.

QCT/FEM can predict vertebral compressive strength ex vivo. We aimed to assess vertebral fracture risk and alendronate effects on osteoporosis in vivo using QCT/FEM. Vertebral strength in 104 postmenopausal women was analyzed, and the discriminatory power for vertebral fracture was assessed cross-sectionally. Alendronate effects were also prospectively assessed in 33 patients with postmenopausal osteoporosis who were

treated with alendronate for 1 year. On the age and body weight adjusted logistic regression, vertebral strength had stronger discriminatory power for vertebral fracture (OR per SD change: 6.71) than areal bone mineral density (BMD) and volumetric BMD. The optimal point for the vertebral fracture threshold was 1.95 kN with 75.9% sensitivity and 78.7% specificity. At 3 months, vertebral strength significantly increased by 10.2% from baseline. The minimum principal strain distribution showed that the area of high fracture risk decreased. At 1 year, the density of the inner cancellous bone increased by 8.3%, while the density of the juxta-cortical area increased by 13.6%. QCT/FEM had higher discriminatory power for vertebral fracture than BMD and detected alendronate effects at 3 months. Alendronate altered density distributions, thereby decreasing the area with a high fracture risk, resulting in increased vertebral strength.

Prediction of proximal femur strength by a quantitative computed tomography-based finite element method -Creation of predicted strength data of the proximal femur according to age range in a normal population and analysis of risk factors for hip fracture-

*Kaneko, M; *Ohnishi, I; *Bessho, M;*Matsumoto, T; *Ohashi, S; *Tobita, K; *Nakamura, K
*Department of Orthopaedic Surgery, University of Tokyo, Tokyo, Japan.
email: ohnishii-dis@ h.u-tokyo.ac.jp

INTRODUCTION

Fall-related fragility fractures in elderly patients with osteoporosis, which can result in severe disability for activities of daily living, is one of the most serious diseases in modern society. However, only 44% of all non-vertebral fractures occur in women with a T-score below 2.5. In men, this percentage is even lower (21%) [1]. However, there is a clear need for the development of more sensitive risk assessment tools, using not only bone densitometry, but also other clinical predictors of fractures. Bone densitometries can explain 60-70% of bone strength and are limited in the ability to account for complex geometry, architecture, and heterogeneity of bone. However, quantitative computed tomography (QCT)-based finite element (FE) methods (QCT/FEM) are able to perform structural analyses taking these factors into consideration to accurately predict bone strength [2-3]. Some preliminary investigations into clinical applications of these methods have been reported [4-5]. To date, however, no basic data have been available regarding predicted strength (PS) by QCT/FEM with reference to age in a normal population. To apply this method for a wide range of clinical uses, a database of PS distributions with reference to age in a normal population is essential. The purpose of this study was thus to create a database on PS values of the proximal femur by QCT/FEM in a normal population as a preliminary trial. With these data, parameters that affect PS value by QCT/FEM were also analyzed.

Materials and Methods

Participants in this study comprised individuals who participated in a health checkup program with computed tomography (CT) at the University of Tokyo hospital from January to December in 2008 and for whom scan data were available for FEM subsequent analyses. The study protocol was approved by the ethics committee in our institution, and each participant provided written informed consent in accordance with the Declaration of Helsinki. Participants included 487 men (mean age, 55.0 years; range, 40-87 years) and 237 women (mean age, 59.0 years; range, 40-83 years). Exclusion criteria included patients with any recent or current disease under treatment with an agent to alter bone turnover or bone metabolism. In addition, subjects were excluded if they had any generalized disease that affects bone metabolism other than osteoporosis (e.g., hyperparathyroidism, hypo-parathyroidism, Paget's disease, renal osteodystrophy, Cushing's disease, steroid-induced osteoporosis, and others), malignant diseases, and rheumatoid arthritis. Scan data of the proximal femur were isolated and taken from overall data from CT of each participant with a slice thickness of 1.25 mm and a pixel width of 0.976 mm obtained using a Light Speed Ultra16 system (GE Yokokawa Medical System, Tokyo, Japan; 120 kV, 80 mAs, 512×512 matrix) with simultaneous scans of a calibration phantom (BMAS 200; Kyoto Kagaku, Kyoto, Japan) containing hydroxyapatite rods. A 3-dimensional FE model was constructed from the isolated data using Mechanical Finder software (RCCM, Tokyo, Japan). FE models were equipped with triangular shell elements with a thickness of 0.4 mm and a size of 3 mm for the outer surface of the cortical bone and tetrahedral solid elements with a size of 3 mm for the rest of the bone. We adopted two loading conditions, comprising stance and fall configurations [6]. Materially nonlinear FE analysis was performed using the Newton-Raphson method. Fracture load was defined as the load when at least one shell element failed. For each participant, height, weight, and abdominal circumference (AC) were measured, and medical history was elicited. Linear regression analysis was used to estimate correlations between age and PS of the proximal femur as analyzed by QCT/FEM. Change in PS with age was also evaluated by grouping participants into 5-year age brackets. One-way analysis of variance was used to compare average PS of participants in each age range. In addition, a multivariate statistical technique was used to determine how PS was affected by age, height, weight, and AC. The software SPSS (SPSS Inc, Chicago, USA), was used for statistical analyses. Differences were considered significant for values of $p<0.05$. For highly correlated variables, variance inflation factor (VIF=1 /(1-R2)), which describes multi-collinearity, was computed. PS of the proximal femur was assigned to a dependent variable, while height, weight, age, and AC were assigned to independent variables. Multivariate statistical analyses were performed using stepwise method. In the analyses, when strongly correlated independent variables were included, they were excluded under a multi-collinearity of VIF≥5.

RESULTS

Average PS of the proximal femur in women was lower than that in men for each age range under both stance and fall loading configurations. PS under stance configuration in men showed a negative significant correlation with age ($p<0.05$), but no correlation with age was found under fall configuration ($p=0.678$). In women, PS showed a negative significant correlation with age under both stance and fall configurations ($p<0.05$). In men, average PS in the 75-79 year range was significantly lower than that in the <64 year range under stance configuration. In women, average PS at 40-44 years was significantly higher than that at >55 years under stance configuration, and was significantly higher than that at >65 years under fall configuration. In men, correlation between AC and weight was very strong with R=0.860. In addition, the VIF of AC was equal to 5.756 but the VIFs of other independent valuables were within a range of 1 to 2, so AC was excluded. In the multivariate analysis of PS in men under stance configuration, the standardized β for height was calculated as 0.045. Because height poorly correlated with PS with $p=0.348$, it was excluded from the analysis. Therefore, the multivariate analysis equation for PS in men under stance configuration was expressed with a standardized β for age of - 0.176 and that for weight of 0.386. Likewise, the multivariate analysis equation in men under fall configuration was expressed with a standardized β for weight of 0.201, that for height of 0.016 ($p=0.760$), and that for age of 0.031 ($p=0.490$). So, height and age correlated poor with PS, and they were excluded from the equation, which was finally expressed by a standardized β for weight of 0.212. In women, the correlation between AC and weight in women was also very strong with R=0.741 but the VIF for AC was equal to 1.874. Thus, both of these parameters could be included in the multivariate analysis equation. In the multivariate analysis of PS in women under stance configuration, the standardized β for height was calculated as 0.113 ($p=0.074$) and that for AC as 0.412 ($p=0.412$). Because height and AC poorly correlated with PS, they were excluded from the analysis equation. Therefore, the multivariate analysis equation for PS in women under stance configuration was expressed with a standardized β for age of - 0.444 and that for weight of 0.331. Likewise, the multivariate analysis equation in women under fall configuration was expressed with a standardized β for height of 0.104 ($p=0.124$) and that for AC of 0.071 ($p=0.944$). Because height and AC poorly correlated with PS, they were excluded from the analysis. Therefore, the multivariate analysis equation for PS in women under fall configuration was finally expressed with a standardized β for age of - 0.407 and that for weight of 0.209. Height did not significantly affect PS in either men or women.

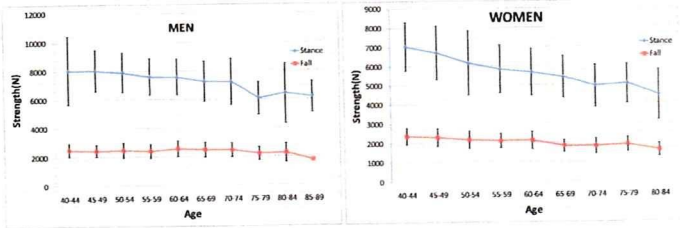

Figure 1: Change in PS of the proximal femur with age

DISCUSSION

This was the first study to investigate changes in PS of the proximal femur by QCT/FEM with age in a normal population. The number of participants in this study was small and may have been insufficient to suggest standard values for PS, but these results still contribute to creating basic standard data for PS in normal people in the future.

This study obtained the following results. First, average PS of the proximal femur was lower in women than in men for all age ranges. Second, PS in men under stance configuration, and those in women under both configurations significantly decreased with age. Third, weight positively affected PS in both men and women. Whether PS by QCT/FEM correlates more closely with fracture risk for osteoporotic patients in comparison to other bone densitometries remains unclear, but the present results did not contradict any existing concept of risk factors for fragility fracture. More baseline data for PS in normal populations need to be accumulated by increasing the number of participants in studies like this. In addition, more factors that affect PS should be analyzed to estimate risk factors for osteoporotic fracture.

REFERENCES:

1. Schuit, S.C., et al., Fracture incidence and association with bone mineral density in elderly men and women: the Rotterdam Study. Bone, 2004. 34(1): p. 195-202.
2. Keyak, J.H., et al., Prediction of femoral fracture load using automated finite element modeling. J Biomech, 1998. 31(2): p. 125-33.
3. Cody, D.D., et al., Femoral strength is better predicted by finite element models than QCT and DXA. J Biomech, 1999. 32(10): p. 1013-20.
4. Imai, K., et al., Assessment of vertebral fracture risk and therapeutic effects of alendronate in postmenopausal women using a quantitative computed tomography-based nonlinear finite element method. Osteoporos Int, 2009. 20(5): p. 801-10.
5. Orwoll, E.S., et al., Finite element analysis of the proximal femur and hip fracture risk in older men. J Bone Miner Res, 2009. 24(3): p. 475-83.
6. Bessho, M., et al., Prediction of strength and strain of the proximal femur by a CT-based finite element method. J Biomech, 2007. 40(8): p. 1745-53.

Strength index by quantitative computed tomography-based finite element method offers higher discriminatory power for hip fracture than areal bone mineral density of the femoral neck

+*Bessho, M; *Ohnishi, I; *Matsumoto, T; *Ohashi, S; *Kaneko, M; *Tobita, K; *Nakamura, K
+*Department of Orthopaedic Surgery, University of Tokyo, Tokyo, Japan
email: ohnishii-dis@ h.u-tokyo.ac.jp

Introduction: The increase in fragility fractures of the proximal femur has become a major problem in our aging society. Accurate assessment of fracture risk and establishment of effective prevention strategies are thus crucial for osteoporotic patients. We established a quantitative computed tomography (QCT)-based finite element (FE) method (QCT/FEM) that is able to more accurately quantify structural strength of the proximal femur compared to previous methods [1]. Previous experimental studies using mechanical testing of cadaver specimens disclosed that strength predicted by QCT/FEM correlated more closely with fracture load than the density value from dual energy X-ray absorptiometry (DXA) or QCT did [2]. However, no previous studies have evaluated the discriminatory power of QCT/FEM for hip fracture. The aim of this study was thus to compare the discriminatory power of QCT/FEM to that of areal bone mineral density (aBMD) and volumetric bone mineral density (vBMD) by conducting a cross-sectional case-control study with osteoporotic women with and without hip fracture.

Materials and Methods: Subjects comprised 41 women aged between 70 and 84 years old who completed a health examination in our institution from January 2008 to December 2008 (non-fracture group), and 30 patients aged between 70 and 84 years old with hip fracture (hip fracture group). Individuals with metallic implants within CT scan area were excluded. The 71 subjects had a mean age of 75.4 years (standard deviation (SD), 4.2 years), mean height of 150.4 cm (SD, 5.5 cm) and mean weight of 51.0 kg (SD, 7.8 kg). The study protocol was approved by our ethics committee and all subjects provided informed consent to participate prior to enrolment. For women without hip fracture, axial QCT was obtained for both the right proximal femur (Light Speed Ultra 16; GE Medical Yokokawa Medical Systems, Tokyo, Japan) (120 kV, 75 mAs, contiguous 2.5-mm thick slices, 512 × 512 matrices) and a calibration phantom (B-MAS200; Kyoto Kagaku, Kyoto, Japan). For patients with hip fracture, axial QCT was obtained for both the contralateral proximal femur (Aquilion Super 4; Toshiba Medical Systems, Tokyo, Japan) (120 kv, 75 mAs, contiguous 3.0-mm thick slices, 512 × 512 matrices) and a calibration phantom within 1 week after fracture. From the QCT data, FE models were created using triangular shell elements with a thickness of 0.4 mm and a size of 3 mm for the outer surface of the cortical bone and tetrahedral solid elements with a size of 3 mm for the rest of the bone [1]. To allow for bone heterogeneity, mechanical properties of each element were computed from the Hounsfield unit value. Ash density for each voxel was determined from the linear regression equation derived by relating the Hounsfield unit of a calibration phantom to the equivalent ash density. Young's modulus and yield stress of each tetrahedral element were calculated using the equations proposed by Keyak et al. [3] and Keller [4]. Poisson's ratio for each element was set as 0.4. Load and boundary conditions were applied to this model to represent two loading configurations, one approximating joint loading during single limb stance (stance configuration (SC)), and the other designed to simulate a fall on the greater trochanter (fall configuration (FC)) [3]. Materially nonlinear FE analysis was performed using the Newton-Raphson method. Predicted fracture load of the proximal femur was defined as the load causing failure at least one plate element [1]. Predicted fracture load was defined as proximal femoral strength index (PFSI). The same QCT scans were used to assess vBMD and aBMD of the proximal femur with commercially available software (QCT Pro; Mindways Software, Texas, USA), referring to the methods described by Bauer et al. [5]. For statistical analysis, the Mann-Whitney test was used to compare PFSI for SC, PFSI for FC, and aBMD and vBMD between groups. A receiver operating characteristics (ROC) curve was drawn to calculate area under the curve (AUC) for PFSI, aBMD and vBMD. Logistic regression analysis was performed to estimate risk factors for hip fracture. For each statistical analysis, differences were considered significant at $p<0.05$.

Results: Women in the non-fracture group had a mean age of 74.7 years (SD, 3.7 years), mean height of 151.2 cm (SD, 4.6 cm) and mean weight of 51.2 kg (SD, 8.0 kg). Patients with hip fracture had a mean age of 76.3 years (SD, 4.7 years), mean height of 149.3 cm (SD, 4.7 cm) and mean weight of 48.4 kg (SD, 7.3 kg). No significant differences in mean age, height or weight were apparent between groups ($p=0.10$, $p=0.14$ and $p=0.12$, respectively). Mean PFSI for the non-fracture group was 4950 N (SD, 1150 N) in SC and 1180 N (SD, 394 N) in FC. Mean PFSI for the fracture group was 3120 N (SD, 547 N) in SC and 980 N (SD, 247 N) in FC. Mean aBMDs for the non-fracture and fracture groups were 0.560 g/cm^2 (SD, 0.112 g/cm^2) and 0.429 g/cm^2 (SD, 0.086 g/cm^2), respectively. Mean vBMDs for the non-fracture and fracture groups were 260 g/cm^3 (SD, 60.4 g/cm^3) and 173 g/cm^3 (SD, 46.8 g/cm^3), respectively. Mean PFSI, aBMD and vBMD were significantly larger for the non-fracture group than for the fracture group ($p<0.0001$ each). The ROC curve is shown in Figure 1. AUCs for PFSI in SC, PFSI in FC, aBMD and vBMD were 0.943, 0.957, 0.836, and 0.879, respectively. AUC for PFSI in SC was not significantly different from that for PFSI in FC ($p=0.75$). AUCs for PFSI in SC and FC were significantly larger than that for aBMD ($p<0.012$, $p<0.005$). AUCs for PFSI in SC and FC were not significantly different from that for vBMD ($p=0.13$, $p=0.07$, respectively). Odds ratio associated with hip fracture per 0.5 SD change adjusted for age, height and weight was 12.0 (95% confidence interval (CI), 3.27-50.6, $p<0.001$) for PFSI in SC, 15.7 (95%CI, 3.20-77.4, $p<0.001$) for PFSI in FC, 2.21 (95%CI, 1.41-3.48, $p<0.001$) for aBMD, and 3.00 (95%CI, 1.72-5.22, $p<0.001$) for vBMD.

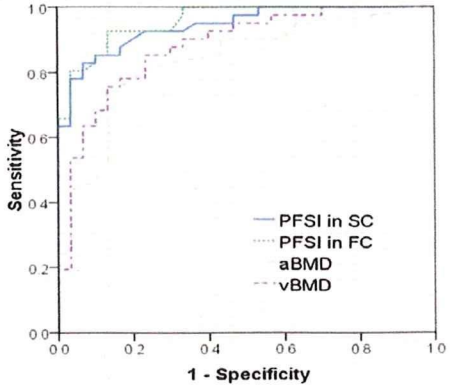

Figure 1: ROC curves showing 1-specificity (false-positive rate) vs. sensitivity (true positive rate) for the PFSI, aBMD and vBMD

Discussion: Risk of hip fracture is reportedly affected not only by decreased femoral neck BMD, but also by morphology of the proximal femur [6]. Evaluation of strength by QCT/FEM takes both BMD and morphology of the proximal femur into consideration, enabling 3-dimensional structural analysis. Strength prediction by QCT/FEM has been reported to accurately predict compressive strength of the proximal femur [2]. In the current investigation, strength index by QCT/FEM offered higher sensitivity and specificity for hip fracture discrimination than aBMD. Orwall et al. reported no significant differences in the discriminatory power for hip fracture between strength index by QCT/FEM and aBMD by DXA. The differences seen in our results may be due to differences in the FEM [7]. The current study was basically a cross-sectional case-control study, but a prospective cohort study will be necessary in the future to investigate the discriminatory power of strength index by QCT/FEM for hip fracture.

References: [1]Bessho, M. et al., J Biomech 2007;40: 1745-53. [2] Cody, D.D. et al., J Biomech 1999;32: 1013-20. [3] Keyak, J.H. et al., J Biomed Mater Res 1994;28: 1329-36. [4] Keller, T.S. J Biomech 1994;27: 1159-68. [5] Bauer, J.S. et al., AJR Am J Roentgenol 2007;188: 1294-301. [6] Faulkner, K.G. et al., J Bone Miner Res 1993;8: 1211-7. [7] Orwoll, E.S. et al., J Bone Miner Res 2009;24: 475-83.

Prediction of Vertebral Strength Under Loading Conditions of Daily Life Using a CT-Based Finite Element Method

+[1] Matsumoto, T; [1] Ohnishi, I; [1] Bessho, M; [1] Ohashi, S; [1]Kaneko, M; [1]Tobita, K; [1]Nakamura, K
+[1] *Department of Orthopaedic Surgery, University of Tokyo, Tokyo, Japan
taqmatsumoto@hotmail.com

INTRODUCTION: Osteoporotic vertebral fractures occasionally occur slowly and asymptomatically, that appear to be caused by loading on the spine during activities of daily living that exceed the vertebral strength of the osteoporotic individual. The most common type of vertebral fracture is reportedly wedge-shaped fracture caused by axial and bending loads. To assess the strength of osteoporotic vertebrae, evaluating vertebral strength under loading as experienced during daily living is important, particularly forward bending. The purpose of the present study was to evaluate differences in predicted fracture strength of vertebral bodies among different loading conditions occurring during activities of daily living using patient-specific finite element (FE) analysis (FEA), which provides accurate prediction of bone mechanics under loading reported by *Imai et al*

PATIENTS AND METHODS: Subjects comprised 41 female patients (mean age, 69.4 years; range, 51-88 years) with postmenopausal osteoporosis according to the guidelines for prevention and treatment of osteoporosis as proposed by the Japanese Society of Osteoporosis (2006 ed.). No subjects had any previous history of disease or use of drugs affecting bone metabolism. The second lumbar vertebra (L2) was examined in these patients, and subjects with previous L2 fracture were excluded. With ethics committee approval, computed tomography (CT) of L2 was performed after obtaining informed consent from each patient. CT of L2 was obtained using a slice thickness of 2 mm with a calibration phantom. CT data were transferred to the workstation, and bone area of the L2 vertebral body was extracted from each scan. FE mesh models were then generated using the advancing front method. An FE model was created with 2-mm tetrahedral elements. Triangular elements with a thickness of 0.4 mm were attached to the model surface. Mechanical Finder software was used to extract bone area and for FE analyses.To allow for bone heterogeneity, mechanical properties of each element were computed from the Hounsfield unit value. Ash density of each voxel was determined from the linear regression equation created by values from the calibration phantoms. Ash density of each element was set as the average ash density of voxels contained in one element. Young's modulus and yield stress of each tetrahedron element were calculated from the equations proposed by *Keyak et al (1998)*. The minimum Young's modulus of each triangular plate was set as 10 GPa. Poisson's ratio of each element was set at 0.4, as used in previous papers. A uniaxial compressive load with uniform distribution was applied on the upper surface of the vertebra, with all elements and all nodes of the lower surface completely restrained. Loading configurations for erect standing and forward bending as described by *Pollintine et al* (2004). were modified and adopted for analysis. Load distribution was divided into three parts: anterior; middle; and posterior. The ratio of load magnitude for each part was assigned on the assumption that the middle part bore the average load magnitude of the anterior and posterior parts. Ratios were thus 19:31:41 for erect standing and 59:48:38 for forward bending. Load was applied on the upper end plate vertically and the lower end plate was fully restrained (Fig. 1).

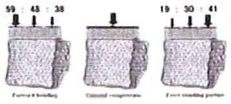

Figure 1: Load and boundary conditions in each model.

Nonlinear analysis was performed using the Newton-Raphson method with a post-yield modulus of 0.05. The ratio of ultimate stress to yield stress was assigned as 0.8. The element crack in tension was defined as occurring when maximum principal stress exceeded element ultimate stress. However, in compression, we introduced both yield and failure. Yield in compression was defined as occurring when Drucker-Prager equivalent stress exceeded element yield stress. Element failure in compression was then defined as occurring when the negative value of maximum principal strain exceeded 10,000 microstrain. Fracture load was defined as the load when at least one element failed. Predicted fracture load in each of the erect standing and forward bending configurations was calculated and compared to that under uniaxial compression. Predicted fracture sites under each loading configuration were also identified. To analyze differences in distribution of fracture sites depending on differences in loading configuration, the whole vertebral body was divided into 3 parts in an antero-posterior direction and 3 parts in a cranio-caudal direction, for a total of 9 parts. Pearson's correlation analyses were performed. Paired analyses among the three groups were performed using the Friedman multiple comparison test. Analysis of differences in distributions of predicted fracture sites was performed using the χ^2 test for all loading conditions. Deviation of the distribution was analyzed by Ryan's method. Differences were considered significant for values of $P<0.05$.

RESULTS: Mean fracture load was 3062 N under uniaxial compression (range, 883-5688 N), 2918 N in erect standing (range, 883-5492 N) and 2693 N in forward bending (range, 883-5296 N). The linear regression equation relating fracture load in erect standing to that under uniaxial compression was expressed as $y = 0.8912x + 19.332$ ($R=0.9522$, $P<0.0001$) (Fig. 2 a). Likewise, the equation relating forward bending to uniaxial compression was $y = 0.7033x + 55.071$, ($R=0.8342$, $P<0.0001$) (Fig. 2 b). Mean fracture load was significantly lower in forward bending than under uniaxial compression ($P=0.00017$).

Figure 2: a)Predicted strengths under uniaxial loading and erect standing. A significant correlation was identified. b) Predicted strengths under uniaxial loading and forward bending. A significant correlation was again identified.

The distribution of predicted fracture sites is shown in Figure 3 for each of the loading configurations. In the cranio-caudal direction, fracture sites tended to be located in the upper third of the vertebral body under all loading configurations. In the antero-posterior direction, the antero-superior part was the most frequent predicted fracture site in forward bending, with76% of all sites. For both erect standing and uniaxial compression, the middle-superior part was the most frequent site (Fig.3). Under all loading conditions, significant differences existed in the distribution of predicted fracture sites. Using Ryan's multiple comparison, the antero-superior part was the most frequent fracture site in forward bending ($P<0.005$).

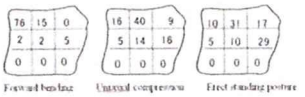

Figure 3: Distributions of predicted fracture sites under each of the loading configurations. Figures were expressed as percentages.

DISCUSSION: Fracture loads in erect standing and forward bending were highly correlated with those under uniaxial compression, however, the correlation between forward bending and uniaxial compression was moderate. Strength in forward bending was significantly lower than uniaxial compression according to Friedman analysis. Thus, when evaluating risk of vertebral fracture, assessment of predicted fracture load would need to be independently determined under each of the loading conditions to fully evaluate fracture risk during activities of daily living. Strength under uniaxial compression is clearly not representative of strengths under other loading configurations. If loading configurations under which the vertebrae are most vulnerable can be determined using CT based FE analysis, atraumatic osteoporotic fractures may be able to be prevented by instructing patients to avoid such postures in activities of daily living. In any case, assessment of fracture risk using a patient-specific CT-based FE method could contribute to preventing vertebral fracture by allowing instruction of patients with predicted high risk to avoid various risky postures during activities of daily living.

References: Imai, K., Spine, 2006, Keyak, J.H., et al. J Biomech, 1998, Pollintine, P., et al., Spine, 2004.

Effect of low-intensity pulsed ultrasound stimulation on gap healing in a rabbit osteotomy model evaluated by micro computed tomography-based 3-dimensional cross-sectional moment and cross-sectional moment of inertia

[1]Tobita, K; +[1]Ohnishi, I; [1]Matsumoto, T; [1]Ohashi, S; [1]Bessho, M; [1]Kaneko M; [1]Matsuyama, J; [1]Nakamura, K
+[1] Department of Orthopaedic Surgery, Faculty of Medicine, University of Tokyo, Tokyo, Japan
ohnishii-dis@h.u-tokyo.ac.jp

INTRODUCTION

Low-intensity pulsed ultrasound stimulation (LIPUS) reportedly enhances restoration of strength at fracture healing sites according to previous experimental studies [1]. However, evaluation of strength by mechanical testing is limited to only one direction, with either bending or torsion. Quantitative micro computed tomography (μCT) is able to acquire 3-dimensional (3D) histomorphometric data and density distributions of hard tissues, from which strength-related parameters can be calculated to allow strength analysis of the tissue. Strength-related parameters such as cross-sectional moment (CSM) and cross-sectional moment of inertia (CSMI) have been used to evaluate strength of the fracture healing site and reportedly correlate well with measured strength from mechanical testing [2]. However, previous studies have performed 2-dimensional (2D) analyses, and 3D evaluations have not been described. The purpose of this study was thus to investigate the effects of LIPUS on osteotomy healing using conducting 3D analyses of strength-related parameters of CSM and CSMI derived from μCT of the osteotomy gap.

MATERIALS AND METHODS

Surgical Procedures and LIPUS Treatment

A total of 42 skeletally mature between 21 and 23-week-old male Japanese white rabbits (Kitayama Labes, Nagano, Japan), weighing 3.4-4.0 kg, were used for this study. Under general anesthesia, four transfixation pins (diameter, 2 mm; length, 50 mm) were inserted at the metaphyseal regions of the tibia in the frontal plane using a custom-made surgical pin driver. Transverse osteotomy was performed using a T-saw (blade thickness, 0.36 mm) with continuous irrigation with saline solution across the mid-shaft of the tibia at 12 mm distal to the tibio-fibular junction. The osteotomy with a 2-mm gap was immobilized with four pins fixed to an external fixator with double side bars.

The LIPUS system (model SAFHS®2000J, Teijin Pharma, Tokyo, Japan), which transmits 200-μsec burst of 1-MHz sine waves repeated at 1kHz with an average intensity of 30mW/cm^2, was used. After postoperative day 3, LIPUS was continued under general anesthesia for both the treatment group (n=7/group/time point) and the control group (n=7/group/time point). The transducer was placed onto the anterior surface of the operated leg with ultrasound coupling gel, for 20 min, six times/week, for 4, 6, or 8 weeks. The control group also received a sham inactive transducer under exactly the same condition as the LIPUS group.

μCT Analysis

All animals were euthanized and the entire tibia was removed. The harvested tibia was scanned by μCT system (Scan X mate-E090, Comscantecno, Kanagawa, Japan). The scan was performed along the long axis of the diaphysis, with a voltage of 60 kVp and a current of 80 mA. Scan range covered 5 mm proximal and 5 mm distal to the center of the gap, with a resolution of 28.57 μm^3 voxel size. The region of interest (ROI) was set at the callus healing area (Fig. 1) defined by the gap filled with callus in 2D CT and extended 0.5 mm proximally and distally to the center of the osteotomy gap with a total of 36 CT axial scans. 3D reconstruction of mineralized tissue was performed using a TRI-BONE system (Ratoc System Engineering, Tokyo, Japan). A threshold for newly formed mineralized callus was set as 200 mg/cm^3. Morphometric parameters used for evaluation were mineralized callus volume (BV, cm^3) and mineralized callus contents (BMC, mg) calculated from the contoured ROI in 3D images, and volumetric bone mineral density of mineralized tissue comprising the callus (mBMD, mBMD = BMC/BV, mgHA/cm^3).

Center of gravity for the ROI was calculated automatically. The *Z* (polar) axis was defined to coincide with the long axis of the tibia. The *Y* axis was defined as parallel to the transfixation pins, which were also parallel to the posterior surface of the tibia (mediolateral (ML) direction). The *X* axis was defined as perpendicular to the *YZ* plane, and was directed anteroposterior (AP) on the tibia (Fig. 2).

Three-dimensional CSM and CSMI

An optional line (I) can be drawn in this *XYZ* coordinate. The angle of the *Z* axis (θ) was measured, and also the degree of angle of the *X* axis (φ) was measured (Fig. 3). The 3D CSM [I (φ, θ)] around this line was calculated as shown. 3D CSM was calculated using the following equation: $I(\varphi, \theta) = \int r^2 dV$ (mm^5), where r is the distance of a voxel to the center of gravity (mm) and dV (BV/voxel) is the area of a voxel (mm^3). The axial CSM was defined as CSMx: I (0, 90), CSMy: I (90, 90), whereas the polar CSM was also defined as CSMp: I (any, 0). We evaluated these three parameters as bone strength indices.

3D CSMI weighted by density distribution was calculated using the following equation: $I'(\varphi, \theta) = \int r^2 dm = \int \rho r^2 dV$ (mg·mm^2), where r is the distance of a voxel to the center of gravity, dm is the measured mineral content of a voxel in callus (BMC/voxel), ρ is the measured volumetric callus mineral density (mBMD), and dV (BV/voxel) is the area of a voxel (mm^3). CSMI x: I' (0, 90), CSMI y: I' (90, 90), and CSMI p: I' (any, 0) were calculated. These three parameters were evaluated as bone strength indices.

Statistical Analysis

The μCT evaluations were analyzed using a one-way ANOVA test. Data were all presented in mean and standard deviation (SD). Statistically significant difference was set at $p<0.05$.

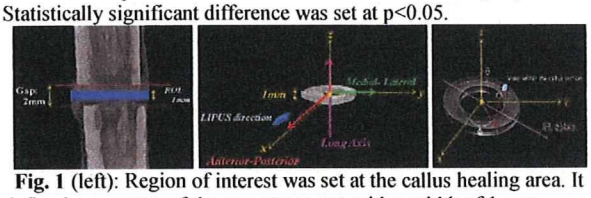

Fig. 1 (left): Region of interest was set at the callus healing area. It defined as a center of the osteotomy gap with a width of 1 mm.
Fig. 2 (middle): The *XYZ* plane was showed. The LIPUS transducer was placed onto the anterior surface of the operated leg
Fig. 3 (right): An optional line (I) can be drawn in this *XYZ* coordinate.

RESULTS

Three-dimensional CSM and CSMI

3D CSMs at the same time point were compared, values for the LIPUS groups were significantly higher than those for control groups for CSMx at 6 weeks ($p < 0.05$) and CSMp at 8 weeks ($p < 0.05$), Fig. 4A.

3D CSMIs at the same time point were compared, values for the LIPUS groups were significantly higher than those of the control groups for MOIx, MOIy, and MOIp at 6 and 8 weeks (Fig. 4B).

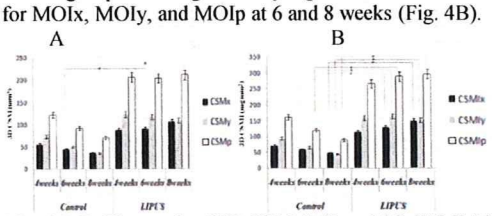

Fig. 4A-B. The result of 3D CSM (left) and 3D CSMI (right) were showed. *= $p < 0.05$.

DISCUSSION

CSM and CSMI are related to architectural strength and show bending and torsion properties. CSMI is a more reliable predictor than CSM for actual bone strength. CSMIp indicates torsional bone property, whereas the axial CSMIs of CSMIx and CSMIy indicate bending properties around the *X* and *Y* axes, respectively. We adopted 3D strength-related architectural parameters derived from μCT scans of the callus to evaluate the effects of LIPUS on restoration of mechanical integrity of the gap healing site.

Our results demonstrate that these bone strength parameters improved with LIPUS during the early phases. However, whether the late phase of callus formation is influenced remains unclear. The present study did not conduct mechanical testing, but μCT scans evaluated strength-related parameters in three independent planes. Mechanical testing can evaluate strength in only one plane for one specimen. Our results demonstrated that LIPUS improves initial restoration of strength at the healing site in bending in AP and ML planes, as well as torsion.

REFERENCES

1. Pilla AA et al, *J Orthop Trauma*, 1990
2. JL Ferretti et al, *J Musculoskel Neuron Interact*, 2001

ACKNOWLEDGEMENT

This project was supported by Teijin Pharma Limited, Tokyo, Japan.

Evaluation of the Accuracy of Articular Cartilage Thickness Measurement by Conventional and Real-time Spatial Compound Ultrasonography

[1]Ohashi, S; +[1]Ohnishi, I; [1]Matsumoto, [1]Bessho, T; [1]Matsuyama, J; M; [1]Tobita, K; [1]Kaneko M; [1]Nakamura, K
+[1] Department of Orthopaedic Surgery, Faculty of Medicine, University of Tokyo, Tokyo, Japan
ohnishii-dis@h.u-tokyo.ac.jp

INTRODUCTION

Articular cartilage thickness has previously been quantified by B-mode ultrasonography [1, 2]. However, cartilage surface and cartilage-bone borders have been decided manually in those studies. In addition, no studies have adopted real-time spatial compound ultrasonography for measuring cartilage thickness. The purpose of this study was to develop a method to objectively quantify articular cartilage thickness in vitro using both conventional and real-time spatial compound B-mode ultrasonography and to evaluate the accuracy of measurement.

MATERIALS AND METHODS

Cartilage samples

Knee joints were obtained for a 6-month- and a 3-year-old pig from a slaughterhouse (Tokyo Shibaura Zouki, Tokyo, Japan), as we assumed that thickness could differ between pigs at different ages. Femoral condyle articular cartilage was used in this study, since cartilage size and shape are relatively similar to those of human knee articular cartilage. After slaughter, whole bodies of pigs were kept at 3 °C in a refrigerated room. On the third day, the hind limbs were detached and sent to our laboratory under the same temperature. In our laboratory, limbs with intact knee joints were packed in plastic bags, degassed manually, sealed hermetically and stored at -20 °C. On the day of the experiment, soft tissues including joint capsules and ligaments were removed after the limbs were thawed in normal saline solution (Otsuka Pharmaceutical, Tokyo, Japan) at room temperature. Osteochondral blocks with the surface size of 20 × 20 mm from the medial femoral condyle were acquired by cutting the bone with a band saw (SWD-250; Fuijiwara Sangyo, Miki, Japan), then fixed on a custom-made acryl sample holder (30 × 30 × 13 mm; Murai & Co., Tokyo, Japan) with resin (GC-Ostron; GC Corporation, Tokyo, Japan). During preparation, samples were continuously cooled and moistened using normal saline solution.

Acoustic measurement

A B-mode 10.0-M Hz linear ultrasound probe (UST-5411; Aloka, Tokyo, Japan) connected to an ultrasound device (Prosound ALPHA 10; Aloka) was attached to a holding arm, which was fixed to a stage with an x,y micrometer for horizontal adjustment to enable identification of the location of cartilage measurement. In the water tank, osteochondral blocks and the transducer surface were placed in 20 °C water. The distance between transducer surfaces and the sample was kept as the transducer focus distance. Edges of the sample were identified by ultrasound signals, and the center of the sample was then identified from those points. B-mode images of the center line of the sample holder were acquired (Fig. 1A). Image settings were for both conventional imaging and real-time spatial compound imaging superimposed with three frames each from a different viewing angle of - 20, 0, and 20 degrees to the right angle. System settings were optimized for imaging the cartilage surface. Brightness line data of 32 points at 0.5-mm intervals in each image were obtained from both the 6-month- and 3-year-old pigs (Fig. 1B). The cartilage surface and cartilage-bone border of the specimen were defined as the peaks of each reflected signal. Cartilage thickness (Tc-US) was measured as the distance between peaks, which was adjusted by the ultrasound speed for each age from our past study [3].

Optical thickness measurement

The specimen fixed to the custom-made sample holder was mounted on a diamond saw device (Minitom; Struers, Westlake, OH), which offers an accuracy of 10 μm for adjustment of the cutting plane. A center-cut plane of the acryl sample holder was created, corresponding to the B-mode ultrasound image plane. Subsequently, each sample was mounted on a glass slide, covered with a cover glass after dripping normal saline onto the sample surface to keep the cartilage moistened and inhibit deformation during measurement due to drying. Cartilage thickness was measured using optical measuring microscopy (MM-400; Nikon, Tokyo, Japan). Using this optical measuring microscopy, points of line data acquisition on the cartilage surface and direction of the US beam were able to be identified from the position and orientation of the acryl sample holder surrounding the cartilage sample. Thickness of the cartilage (Tc) along the beam direction was measured at each point.

Mean and standard deviation (SD) of Tc for each sample were calculated. Linear regression analysis was performed and Pearson's coefficient of correlation was used to compare Tc-US to Tc. A correlation was considered significant for values of $p<0.05$.

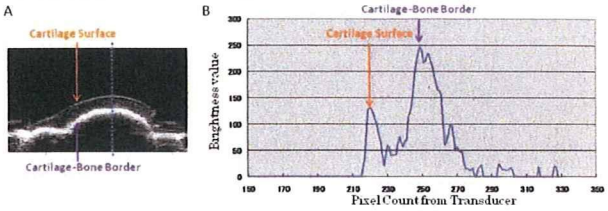

Figure 1: A) B-mode ultrasound image of the sample is shown. **B)** Line data acquired from the dotted line in the ultrasound image (A). Peak of the reflected ultrasound signal were defined as the surface and border of the tissue.

RESULTS

In all B-mode line data, peaks of reflected ultrasound signals from the cartilage surface and cartilage-bone border were clear enough to be identified. Mean Tc and Tc-US (conventional, spatial compound) for both samples are shown in Table 1. Tc-US was significantly correlated with Tc in both the 3-year- and 6-month-old pigs ($p<0.0001$ each) (Fig. 2). Pearson's coefficient of correlation tended to be slightly higher with spatial compound in each sample.

	6-month-old pig	3-year-old pig
Tc (mm)	2.40 ± 0.39	1.49 ± 0.10
Tc-US (conventional)	2.46 ± 0.42	1.45 ± 0.18
Tc-US (spatial compound)	2.40 ± 0.47	1.47 ± 0.14

Table 1. Mean Tc and Tc-US (mm). Values are provided as mean ±SD.

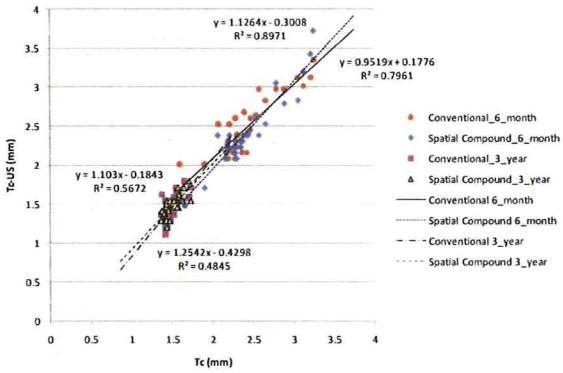

Figure 2. Scatter plot of each ultrasound image setting and sample. Linear regression analysis shows good agreement between Tc and Tc-US in all plots.

DISCUSSION

This is the first study to measure Tc using real-time spatial compound ultrasonography, which has been adopted in evaluating other tissues, such as tendon [4] and ligament [5]. From our results, real-time spatial compound ultrasonography may potentially have higher accuracy for measuring Tc than conventional methods, even though both showed good accuracy in our study. We believe the accuracy of our method is sufficiently high to allow application to measure human Tc in future studies.

REFERENCES:

[1] Myers et al. J Rheumatology, 1995; 22; 109-16.
[2] Burkhard et al. Arthritis & Rheumatism, 2009; 61; 435-41.
[3] Ohashi et al. 55th Orthopaedic Research Society, 2009.
[4] Bartolotta et al. Radiol Med. 2007 ; 112 ; 562-71.
[5] Sorrentino et al. Radiol Med. 2009 ; 114 ; 312-20.

ACKNOWLEDGEMENT:

This work was funded by the grant in aid of the Comprehensive Research on Aging and Health H19-007 of the Health and Labour Sciences Research Grants from the Ministry of Health, Labour and Welfare of Japan.

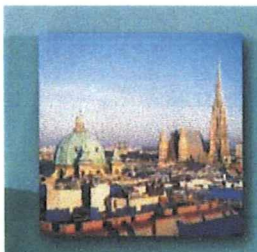

EFORT 10th Congress of the European Federation of National Associations of Orthopaedics and Traumatology

VIENNA, AUSTRIA
3 - 6 June 2009

Free Papers
E-Poster
Symposia
Instructional Lecture
Controversial Case Discussions
Guest Societies
ExMEx
Comprehensive Review Course
Satellite Symposia
Index of Authors
Time Table

Search

E-Poster Content

CLOSE SESSION

Presentation	Pid	Title
	P1841	Prediction of strength and fracture location of the proximal femur by a CT-based nonlinear finite element method - Effect of load direction on hip fracture load and fracture site -

Authors

Masahiko Bessho, Isao Ohnishi, Takuya Matsumoto, Satoru Ohashi, Kenji Tobita, Masako Kaneko, Juntaro Matsuyama, Kozo Nakamura

Abstract

Abstract: Introduction: In the clinical application of CT/FEM, strengths of the proximal femur and lumbar vertebrae are most frequently evaluated. No other CT/finite element model that can be applied to both the proximal femur and the vertebrae has been reported. Therefore, data were unavailable regarding correlations between femoral and vertebral predicted fracture loads (PFLs). One of the purposes of the present study was thus to validate our model by comparing PFLs in our model to fracture loads derived from mechanical testing in previous studies. The other goal was to clarify whether either femoral or vertebral strength in postmenopausal osteoporosis patients is predictable by CT/FEM of only one of the two sites. We thus investigated whether femoral PFL could be utilized to estimate vertebral PFL. Materials and Methods: Right femur and the second lumbar vertebra (L2) in 40 female patients with postmenopausal osteoporosis (average: 70.1) were evaluated. The study protocol was approved by our ethics committee. Axial CT scans of the proximal femur and L2 were obtained (slice thickness: 3 mm (femur), 2 mm (L2)) as well as scans of a calibration phantom. The CT data were transferred to a workstation and 3D finite element models were constructed from the CT data using the software that was developed by the authors (bessho et al. 2007). Load and boundary conditions were applied to this model to represent two loading configurations, one was approximating joint loading during single limb stance (stance configuration: SC), and the other loading configuration was designed to simulate a fall on the greater trochanter (fall configuration: FC). A uniaxial compressive load with uniform distribution was applied on the upper surface of the vertebra and all the elements and all the nodes of the lower surface were completely restrained. Correlations among PFLs of the femur (in SC and FC) and the L2 were investigated. Pearson's correlation analysis was used and the significance level was set as p values of less than 0.05. Result: The average PFL of the proximal femur in SC was 3910 N (SD: 719 N), 1290 N (SD: 323 N) for FC, respectively. The average PFL of L2 was 3010 N (SD: 1110 N). The correlation coefficient relating PFL under SC to that under FC was 0.647 ($p < 0.001$). The correlation coefficient relating PFL under SC to vertebral PFL was 0.472 ($p < 0.01$). no significant correlation was noted between femoral PFL in FC and vertebral PRL (p=0.10). Discussions: Our results did not contradict these previous studies (Eskstein et al. 2002, Mcbroom et al. 1985). PFL in FC may well correlate to vertebral PFL in Japanese women with postmenopausal osteoporosis. In our study, femoral PFL in SC could be utilized to estimate vertebral PFL and femoral PFL in FC.

General orthopaedics
Sports / knee soft-tissue
Hip
Knee osseous
Trauma / polytrauma
Spine (including trauma)
Shoulder / elbow
Hand / wrist
Foot / ankle
Paediatrics
Bone and Joint Tumor
Infection
Osteoporosis
Pain control / rehabilitation and non-surgical management
Basic science

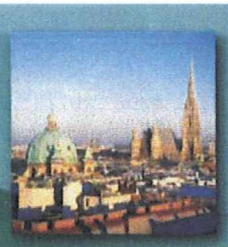

EFORT 10th Congress of the European Federation of National Associations of Orthopaedics and Traumatology

VIENNA, AUSTRIA
3 - 6 June 2009

Free Papers
E-Poster
Symposia
Instructional Lecture
Controversial Case Discussions
Guest Societies
ExMEx
Comprehensive Review Course
Satellite Symposia
Index of Authors
Time Table
Search

E-Poster Content

CLOSE SESSION

Presentation	Pid	Title
	P2006	Evaluation of Measurement Precision for Articular Cartilage Ultrasound Speed by Time of Flight Method

Authors

Satoru Ohashi, Isao Ohnishi, Takuya Matsumoto, Masahiko Bessho, Juntaro Matsuyama, Kenji Tobita, Masako Kaneko, Kozo Nakamura

Abstract

Ultrasound speed in articular cartilage needs to be determined for morphological evaluation of cartilage using ultrasonography. The purpose of this study was to develop a method of measuring cartilage ultrasound speed and to evaluate the precision of our original measurement method. Knee joints of a 6-month-old pig and a 3-year-old pig were obtained from a slaughterhouse. The hind limbs were detached and sent to our facility under 3 °C. The limbs with intact knee joints were packed in plastic bags, degassed manually, sealed hermetically and stored at -20 °C. On the day of the experiment, soft tissues were removed after the limbs were thawed in normal saline solution at room temperature. Osteochondral blocks from the medial femoral condyle were acquired by cutting the bone with a band saw, then fixed on a custom-made acryl sample holder (30 x 30 x 13 mm; Murai & Co., Tokyo, Japan) with resin. A radiofrequency (RF) signal-acquiring system equipped with a 10.0-MHz pulse-echo transducer (diameter, 13 mm; radius of curvature, 60 mm; model V311-SU; Olympus NDT, Waltham, MA) connected to a pulser/receiver (NDT-5800; Olympus NDT) was used for measurements. The transducer and sample holder were attached to a custom holding assembly, which has an adjustment stage to enable identification of the location of cartilage measurement. In the water tank on the stage, osteochondral blocks and the transducer surface were placed in 20 °C water at the transducer focus distance. RF signals were recorded using an oscilloscope (DPO4034; Tektronix Japan, Tokyo, Japan). RF signals of 9 points at 1-mm intervals at the center of the sample were obtained from both the 6-month-old and 3-year-old pigs. Time of flight (TOF) was defined as the duration (?t) between peaks of RF signal envelope, corresponding to the travel time of the US pulse back and forth between the cartilage surface and cartilage-bone border of the specimen. The specimen fixed to a custom sample holder was mounted on the diamond saw device (Minitom; Struers, Westlake, OH). Thickness of the cartilage (Tc) along the beam direction was measured at each point using optical measuring microscopy (MM-400; Nikon, Tokyo, Japan) and ultrasound speed in cartilage (USc) at each point was calculated: USc = (2×Tc)/?t. Mean ultrasound speed in cartilage from the 9-point measurement was 1488 ±48 m/s (mean ±SD) for the 6-month-old pig and 1709 ±104 m/s for the 3-year-old pig. With Student's t-test, ultrasound speed of the cartilage was significantly higher for the 3-year-old pig than for the 6-month-old pig ($p<0.0001$). The coefficient of variance (CV) for precision evaluation of this ultrasound speed measurement was 3.1% for the 6-month-old pig and 5.5% for the 3-year-old pig. We believe the precision of our method is sufficiently high to allow application to measure the ultrasound speed of human cartilage in future studies.

General orthopaedics
Sports / knee soft-tissue
Hip
Knee osseous
Trauma / polytrauma
Spine (including trauma)
Shoulder / elbow
Hand / wrist
Foot / ankle
Paediatrics
Bone and Joint Tumor
Infection
Osteoporosis
Pain control / rehabilitation and non-surgical management
Basic science

Title

Fracture reduction robot for safe and accurate fracture reduction of hip fracture.

Authors and Institution

Sanghyun Joung[1], Hongen Liao[1], Shinya Onogi[1], Mamoru Mitsuishi[1], Yoshikazu Nakajima[1], Nobuhiko Sugano[3], Masahiko Bessho[2], Satoru Ohashi[2], Takuya Matsumoto[2], Isao Ohnishi[2], Ichiro Sakuma[1]

[1]Graduate School of Engineering, the University of Tokyo, Japan,

[2]Graduate School of Medicine, the University of Tokyo, Japan,

[3]Graduate School of Medicine, Osaka University, Japan

Abstract

Hip fracture is a fracture in the proximal end of the femur. Most patients with hip fracture are treated operatively. In the case of displaced fractures, the fracture should be reduced before fixing the bone fragments. The first part of the procedure is the reduction of the fracture in the AP view by using longitudinal traction. Over distraction of the fracture must be avoided, as this may damage the femoral head vascularity. Next is the reduction in the lateral view by the internal rotation of the foot. Surgeons must exert a large force while pulling on the inferior branch and there are no safe methods available to avoid excessive force being put on the injured limb. This paper introduces a fracture reduction robot that has a high accuracy and reliable safety for assisting with hip fracture reduction.

The fracture reduction robot has six degrees of freedom (i.e, three DOFs in translation and three DOFs in rotation) of which precision are 1μmm in translation and 1μrad in rotation. For an accurate fracture reduction, the bone fragment is directly connected to the robot with the customized jig so that its position can be controlled precisely by the fracture reduction robot.

In order to limit the reduction force within the safe ranges, two mechanical failsafe modules are installed; one is for a traction direction and the other is for the internal or external rotation. The structure of two mechanical failsafe modules has a plunger style with a still-made roller pushed into a hollow by a spring. The threshold can be adjusted by changing the spring compression force. The software force limiter is also designed to prevent the excessive reduction force. Two thresholds are used not only to avoid the sudden stopping motion of the robot, but also to forewarn an operator of an increase in the reduction force by decelerating the robot. Two thresholds of the software force limiter are set smaller than the threshold force of the mechanical failsafe modules so that the mechanical failsafe is only operated when the software problem occurs.

The robot can rotate the bone fragment centering on one point of the bone fragment; this can reduce the movement of the soft tissues around the bone fragments. The algorithm is as follow: The method supposes that the force and moment given to the bone fragment by the surgeon is the movement direction intended by him. Then, the movement of each axis is calculated considering the bone fragment and the robot as a rigid body. One force sensor is installed to measure the force given to the bone fragment. The navigation system that has a function of 2D/3D registration will be used to determine the bones' coordinates.

The clinical usefulness of the safety features and the operation mode of the robot are evaluated with the simulated fracture reduction of a hip fracture model. Tests were conducted eight times. The reduction forces were recorded during the fracture reduction and the reduction results are evaluated from parameters related to the mechanical axis used to assess the femur deformity. The reduction force can be reduced within the set threshold of the software force limiter and the fracture model can be reduced within differences of 2 degrees and 2 mm comparing with the normal values. The fracture model could be accurately reduced with reliable safety.

Title

Force estimation acting on fixation screws for a safe direct fracture reduction.

Authors and Institution

Sanghyun Joung[1], Hongen Liao[1], Shinya Onogi[1], Mamoru Mitsuishi[1], Yoshikazu Nakajima[1], Nobuhiko Sugano[3], Masahiko Bessho[2], Satoru Ohashi[2], Takuya Matsumoto[2], Isao Ohnishi[2], Ichiro Sakuma[1]

[1]Graduate School of Engineering, the University of Tokyo, Japan,

[2]Graduate School of Medicine, the University of Tokyo, Japan,

[3]Graduate School of Medicine, Osaka University, Japan

Abstract

Most hip fractures are treated by operatively. With the displaced fracture, the fracture must be reduced before the fixation of the bone fragments. Surgeon handles an ankle in order to reduce the fracture. This is an invasive reduction method, but it is difficult to locate the bone fragments precisely. Thus, a direct reduction method is sometimes required for more accurate reduction in case of the complex fractures or a robot assisted fracture reduction. Two external fixation screws are inserted into the bone fragment in order to fix the bone fragment with a direct reduction method. And the two screws are connected to the handle like a ring or a half ring frame. With this method, the bone fragment may be damaged or a secondary fracture incurred by these screws subject to the weight of the patient's own leg and the resistive force against the reduction force. Therefore, it is important to monitor the force acting on a screw during the direct fracture reduction. This paper presents the estimation method of the pull-out and bending force acting on the fixation screws in real-time using the characteristic matrix, which expresses the material property, mechanical structure, the deformity, and more.

A force sensor of 6 degrees of freedom with handle is installed on the ring frame. However, due to the complex structure of the connection between the bone fragment and the fixation screws, the force distribution cannot be calculated easily using one force sensor. To solve the problem in real-time with a finite element analysis, it is assumed that the problem is linear, which means the outputs can be estimated from the previously calculated result. The method follows:

1. Two external fixation screws are inserted into the bone fragment.
2. The coordinates of the two screws and the force sensor are measured.
3. The coordinate information is input into the previously prepared CAD data that already have the material properties.
4. The characteristic matrix that defines the relation of inputs-force sensor- and outputs-force acting on two fixation screws-are calculated using the finite element analysis.
5. The applied forces to the screws are calculated in real time by multiply the measured force by the force sensor to the characteristic matrix during the fracture reduction.

The method is evaluated using a celluar rigid polyurethane foam block-density: 0.2g/cc- instead of the bone fragments. Two more force sensors are installed to measure the real force that is applied two fixation screws. The estimated forces by the proposed method and the measured forces by two additional force sensors are compared and correlations are calculated.

The evaluation results show the high correlation of pull-out force-0.87 at screw1 and 0.96 at screw2-, but the correlation of the resulting moments are low-0.65 at screw1 and 0.56 at screw2-. The simulation model used in this study has two limitations. First, the two fixation screws are fixed only at a point. The other thing is that the weight of the partial part is not considered. These cause a low correlation in the moment analysis. The resultants can be influenced by the loosened fixation of screws and the bone strength. It is, however, highly unlikely that the fracture is reduced with the loosened fixation of screws in clinical case. The influence of the weaken bone strength can be evaluated using the celluar rigid polyurethane foam that has a low density. To actually use the proposed method, the tight connection between the bone and the screw must be guaranteed, and a more precise analysis model is required; this is future work.

骨折整復支援ロボットの拘束動作の評価

○鄭常賢，廖洪恩，小林英津子，光石衛，中島義和，菅野伸彦[a]，別所雅彦，
大橋暁，大西五三男，佐久間一郎（東京大学，[a]大阪大学）

Evaluation of spatial constraint of a fracture reduction assisting robot

*Sanghyun JOUNG, Hongen LIAO, Kobayashi ETSUKO, Mamoru MITSUISHI,
Yoshikazu NAKAJIMA, Nobuhiko SUGANO[a], Masahiko BESSHO, Satoru OHASHI,
Isao OHNISHI, Ichiro SAKUMA, (the University of Tokyo, [a]Osaka University)

Abstract − We have developed a fracture reduction assisting robot for a hip fracture. A bone fragment is directly connected the robot using two external fixation screws for more precise positioning. We devised a manual control mode of the robot; which can assist in power and constrain a rotation center of the bone fragment. Movement of the rotation center was traced using the 3D optical measurement system. The resultants show that the proposed method has average error within 2mm though its maximum error is over 2mm. The error is mainly due to the play of the rotation axes of the robot. We will fix the mechanical fault and add in the more robust control method.

Key Words: Surgical robot, Fracture reduction, Spatial constraint, Power assistance

1. 背景

股関節骨折は大腿骨の骨盤側末端の骨折である．手術による治療が多く行われ，手術は折れた骨片を固定する前に骨片を元の位置に戻す骨折整復が行われる．従来の股関節骨折の整復は足首を持ち整復を行う介達式整復で，侵襲はないものの足首に与えられた整復力が関節，軟部組織に吸収され骨片の精確な位置操作が難しい．また，骨片の牽引は術者へ負担が大きく，牽引力を補助する牽引台が多く使用されるが，その自由度が足らず正確な整復は難しい．そこで，我々のグループでは整復力を補助しながら正確な整復を目指し，ロボット支援骨折整復に関する研究を進めている．これは，従来のように足首をもち整復を行う介達式整復をより正確に行うための研究と[1]，多少侵襲は発生するが，骨片に二つの創外固定ピンを挿入，そのピンをロボットと固定し，整復を行う直達式整復によるものがある．直達式では既にナビゲーションによるモデル骨の自動整復を行った[2]．術者がロボットを動かす手動モードに関してもその制御方法を発表したが[3]，その結果が要求仕様を満たしていなかった．また，ロボットの改良を行ったので報告する．

2. 方法

2.1 骨折整復支援ロボット

骨折整復支援システムは骨折整復支援ロボット(以下整復ロボット)とナビゲーションシステムに構成されている．ナビゲーションシステムは骨片間と整復ロボットとの位置関係を追跡し，骨片のゴール位置と整復パスを計算する．整復ロボットは骨片と繋がり正確に骨片を動かす役割をする．

図 1(a)に整復ロボットの外観を，図 1(b)にその動きを示す．ロボットは 6 自由度を持ち，そのうち 3 自由度は並進方向，3 自由度は回転方向である．牽引方向のボールスプライン構造にすることで撓みをなくし軽量化を図った．回転 3 軸は一点で交わる構造にして制御を簡便にした．

骨片と整復ロボットとの連結様子を図 2 に，その手順は以下に示す．まず，二つの創外固定ピンを挿入しリングフレームに固定する．整復ロボットには 6 自由度を持つ専用の固定ジグを取り付けリングフレームと繋げる．

骨折整復システムの臨床使用は 3 段階として考えている．先ずは，従来式の骨折整復にナビゲーションシステムの導入である．次は，整復ロボットの手動モードの導入であり，ナビゲーションシステム或いは放射線画像をみながら術者の操作による骨折整復である．最後にはナビゲーションシステムと整復ロボットとの統合による自動骨折整復方式を導

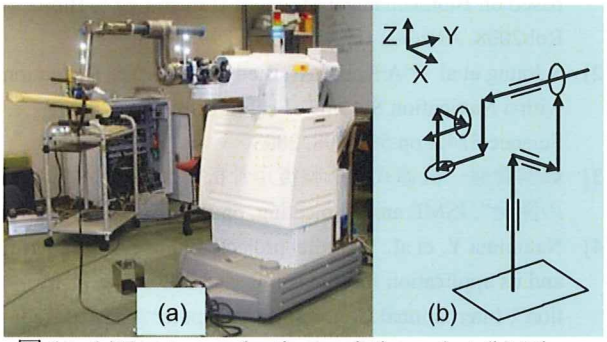

図 1. (a)Fracture reduction assisting robot (b) Kinematics of the robot

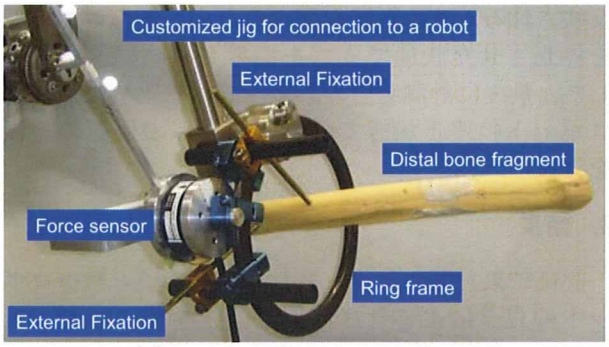

図 2. Direct bone connection

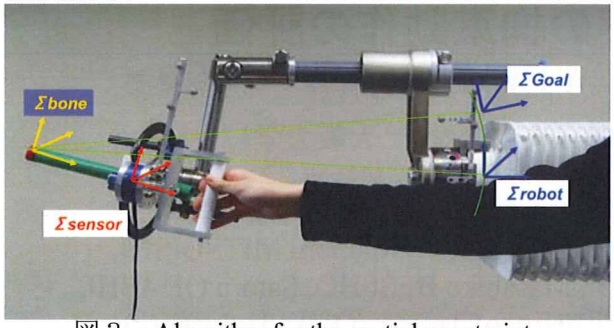

図３．Algorithm for the spatial constraint

入する．今回は整復ロボットによる手動整復に関して詳しく述べる．

2.2 整復ロボットによる手動整復

整復ロボットは整復力の補助だけではなく，骨片の動作空間を拘束する機能を実装した．これは，骨片の長軸に沿って骨片を牽引したり長軸周りに回旋させたりすることを可能とする．骨折面の一点を中心に骨片の回転させることは安全面でも重要なことであり，骨折部位の周辺組織の変位を減らす効果がある．

整復ロボットの制御方法を図に示す．術者は取っ手を持ち，骨片を動かす．取っ手とリングフレームの間には力センサがあり，術者が入れた力を計測する．力センサの入力値は骨片座標での力で変換する．そのとき，骨片座標系での力，モメント方向を術者が骨片を動かそうとした方向としてその大きさを変位量として仮定して骨片のゴール位置を計算する．骨片と整復ロボットを固体として考え，骨片のゴール位置から整復ロボットのゴール位置を計算する[3]．骨片座標の設定はナビゲーションシステムの2D/3Dレジストレーション方法を使用する見込みである[4]．

2.3 評価方法

光学式位置計測装置(Polaris,)を使い，骨片(Σbone)，力センサ(Σsensor)と整復ロボット(Σrobot)の座標を設定した．骨片座標の原点を中心に±15°程度回転しそのときの骨片座標の原点の位置を整復ロボット座標系で記録した．動作空間が正しく拘束されたら，骨片を動かしても骨片座標の原点は固定されるはずなので，最初の骨片座標の原点の位置からの変位を誤差として計算する．整復ロボットは直列構造であるため，軸の遊びなどが先端で大きく反映される．その影響を調べるため，整復ロボットを停止させた状態で先端を揺らしその動きを記録した．最後に計測装置の誤差を調べるために，整復ロボットの停止状態で骨片座標原点の位置の記録を行った．

3. 結果

評価結果を図に示す．横軸は制御誤差と整復ロボットのガタによる骨片原点の動きを整復ロボット座標系の各軸に分けたものである．縦軸には誤差の

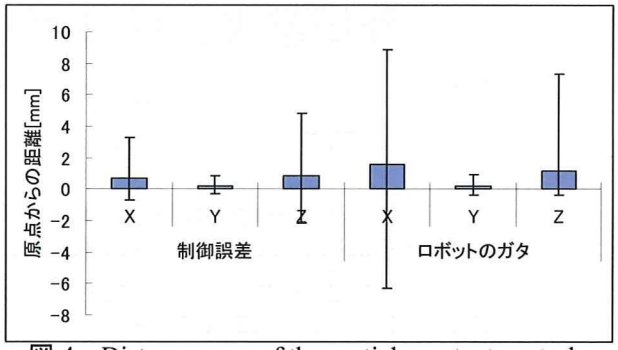

図 4. Distance error of the spatial constant control

平均と原点からの±最大距離を示す．光学式位置装置の誤差はX軸方向(計測機の奥行き方向)の誤差が多く，RMSで0.05mmであった．計測機のYとZ軸の誤差は何れも0.01mmであった．制御誤差，ガタによる動き共にX，Z軸が大きい変位を見せ，Z軸に関してはプラス方向(自重の反対方向)に偏っていることがわかる．

4. 考察と結論

骨折整復の整復力を支援するロボットを開発し，空間拘束が可能な制御方法を提案，評価した．整形外科では一般にあらゆる評価値が2mm, 2°以下であることが望ましい．空間拘束制御の結果，誤差の平均は2mm以下であったが，その最大値は2mmを超えている．誤差の原因は以下のように考えられる．

- 座標系を設定するときに生じる光学式位置計測装置の誤差によるもの．
- 整復ロボットの回転軸が持つガタによるもの．
- オープン制御を行ったことからのもの．

座標系設定による誤差は平均値を取ることにより小さく出来る．制御誤差がガタによる動きよりも小さいのは，整復ロボットを動かすために入れた力は20N程度であるが，最大のガタを発生するのに必要な力は60N程度であったためである．骨片座標の原点はロボット座標の原点から780mmはなれたところで位置したとこからX，Z軸のガタを見積るとX軸で1.4°，Z軸が0.5°である．今後整復ロボットの機械的問題を検討し，ロバスト制御を組み込む予定である．

参 考 文 献

[1] T. Douke et al.: “Control of Fracture Reduction Robot based on Biomechanical Model of Human Leg” , Bio-Rob2008, Arizona, USA, pp. 295-299, 2008

[2] S.Joung et al. : “A Robot Assisted Hip Fracture Reduction with a Navigation System”, Lecture Note in Computer Science 5242, pp.501-508, 2008

[3] 鄭常賢他: “直達式骨折整復用骨折整復支援システムの開発”, JSME annual meeting, pp.517-518, 2007

[4] Nakajima Y. et al.: “Parallel projected light field rendering and its application for intensity-based 2-D/3-D registration”, International Congress on Computer Assisted Radiology and Surgery (CARS) 2009, Berlin, Germany

直達式骨折整復支援システムの開発

○鄭常賢(ジョン　サンヒョン)　工学系研究科精密機械工学専攻
小林　英津子　工学系研究科精密機械工学専攻
中島　義和　工学系研究科バイオエンジニアリング専攻
光石　衛　工学系研究科産業機械工学専攻
大西　五三男　医学部整形外科
佐久間　一郎　工学系研究科精密機械工学専攻

高齢者に起こり易い大腿骨頚部骨折の治療法は外科的な手術によるものがほとんどである．手術では大腿骨の遠位骨片を牽引しながら整復し，ピンによって固定する．しかし，大腿筋などの周辺組織が萎縮した状態では整復のための牽引に大きな力が必要となるため術者にとって負担となる．また，X 線透視下で 2 次元の情報を用いて位置決めを行わなければならないため，術者の熟練が必要であり，手術を行うことで術者が受ける X 線被爆も問題である．

これらの問題に対し，我々は骨折整復支援システムを開発した．システムは骨折整復ロボットとナビゲーションシステムに構成されている．このシステムではロボットを使う利点を活かすため骨片にピンを打ち，ピンに連結されたリングを持って直接整復を行う直達式骨折整復方法を用いる．

骨折整復ロボットは並進 3 自由度と回転 3 自由度の 6 自由度を有する．骨片の牽引と回旋をするときの整復力が設定値より大きくなると各関連軸をフリーにするフェイルセイフ装置が装着されており安全性を保つ．ソフトウェアレベルでは整復力に対してロボットの速度を減らす手法で安全性を高める。動作モードは術者の整復力補助する手動モード，ナビゲーションからの指令により自動で整復を行う自動整復モードがある．

手動モードでは，骨片の大きな姿勢変化を防ぐため，骨片座標系でロボットを動かせるようにロボットの制御をする手法を提案しその精度評価を行った．

ナビゲーションシステムは術前に作成した CT からの 3 次元モデルを用いて整復ゴールを計算する．術中には C-arm で撮った画像と 3 次元モデルをレジストレーションすることにより，実空間での骨片間の位置関係を認知する．骨片の現在位置からゴールまでの整復パスは術者の意見を反映して作成され，整復ロボットに指令を送り整復を行う．開発したシステムにて骨折モデルでの整復実験を行い，その有効性を示す．

統計形状モデルを用いた骨折骨の位置姿勢および形状の推定

○斎藤季[a]，成田拓也[a]，中島義和[ac]，橋詰博行[b]，小野木真哉[c]，杉田直彦[a]，
藏本孝一[d]，中島義雄[d]，光石衛[a]

[a]東京大学大学院工学系研究科

[b]笠岡第一病院

[c]東京大学インテリジェント・モデリング・ラボラトリー

[d]ナカシマメディカル株式会社

Fractured bone position and shape estimation based on the 2-D/3-D registration of a deformable model

T. Saito[a], T. Narita[a], Y. Nakajima[a], H. Hashizume[b], S. Onogi[c], N. Sugita[a], K. Kuramoto[d], Y. Nakashima[d], M. Mitsuishi[a]

[a] School of Engineering, University of Tokyo, Tokyo, Japan

[b] Kasaoka Daiichi Hospital, Okayama, Japan

[c] Intelligent Modeling Laboratory, University of Tokyo, Tokyo, Japan

[d] Nakashima Medical Co., Ltd., Okayama, Japan

Abstract: Two-dimensional/three-dimensional (2-D/3-D) registration is a promising method for determining the coordinate transformation matrix between pre-operative space and intra-operative surgical space. It usually requires intraoperative X-ray fluoroscopy and preoperative computer tomographic (CT) imaging, and costs X-ray exposure to patients. Deformable model based 2-D/3-D registration methods have been proposed in order to estimate bone position and shape on intra-operative surgical space without CT imaging. However these deformable models are generated by normal bones, and it is hard to estimate the original bone shape from fractured bone X-ray images. In this paper, we propose a deformable model based 2-D/3-D registration method which supports fractured bones. In our experiments for hand bone fracture, the estimation error of shapes were reduced from 14.7% to 12.6% and the stability of calculation was improved.

Keywords: hand surgery, surgical navigation, 2D/3D registration, statistical shape model, scaphoid bone

1. 背景

舟状骨は手首部分を構成する骨の一つである．舟状骨を骨折時には舟状骨骨折整復手術が行われるが，現在この手術において，手術の安全性向上と高精度化を目的とした，舟状骨への術具刺入を自動で行う手術ロボットの開発が行われている．手術ロボットを使用するには，ロボットに対する患部の位置姿勢を求めるレジストレーションが必須である．本システムではレジストレーションに2D/3D レジストレーション法を使用し，骨の位置姿勢を推定する．2D/3D レジストレーションは，術前撮影骨 CT 画像と術中撮影 X 線画像内の骨輪郭を対応付けすることで実現される．しかし，骨 CT モデル作成に必要な X 線 CT の撮影は医療コストが高く，また患者の X 線被曝量が多い．

高村らの研究[1]において，X 線 CT を使用しない骨の位置姿勢推定手法が提案された．この手法では骨 CT モデルに代わり統計形状モデル[2]を使用し，2D/3D レジストレーションを用いた骨の位置姿勢推定及び形状推定を同時に行う．統計形状モデルとは，複数の骨の形状から，一つの平均形状と複数の統計的な変形を記述したもので，形状パラメータを変化させることで，各個人の骨形状を表す．しかし，高村らの手法では，骨折時の X 線画像を考慮していないため，本研究の目的とする骨折整復手術への応用には不十分である．そこで本研究では，骨折時に対応した舟状骨の位置姿勢および形状の推定手法を提案する．

2. 手法

統計形状モデルの作成，そして 2D/3D レジストレーションを用いた骨形状と位置姿勢の推定の 2 段階からなる．詳細を以下に述べる．

2.1 統計形状モデルの作成

統計形状モデルの作成には，まず，複数の CT 画像から骨の表面形状を抽出し，サーフェイスモデルを作成する．次に，座標系の規格化を行い，各サーフェイスモデルの座標系を統一する．サーフェイスモデルの内側に含まれるボクセルに対して平均位置を原点とした主成分分析を行い，第 1 主成分軸から順に X，Y，Z 軸とする．次に，一つのサーフェイスモデルを基準モデルとし，基準モデルに対してすべてのサーフェイスモデルの位置合わせとスケールの調整を Iterative Closest Point 法[3]を用いて行う．その後，基準モデルの polygon を形成する各頂点から各サーフェイスモデルの各 polygon を形成する点群に対して最近傍点探索を行い，最近傍点を各頂点の対応点とする．最後に，設定した対応点の頂点の座標値について主成分分析を行う．統計形状モデルは次式で表される．

$$V = \overline{V} + \sum_{i=1}^{N} P_i b_i \qquad (1)$$

ここで，V は統計形状モデル，$\overline{V}$ は平均形状，Pi は主成分ベクトル，bi は変形パラメータ，N は主成分数である．

2.2 2D/3D レジストレーションによる骨形状およ

び位置姿勢の推定

本手法では2D/3Dレジストレーションに用いる輪郭情報は骨折部の数だけ存在し，それらを拘束条件として骨折前の骨形状及び各骨片の位置姿勢を推定する．以下に手順を示す(Fig. 1).

(1) 骨折した骨のX線画像撮影を行う．
(2) 撮影した骨の輪郭線を手動で抽出する．これは骨折時に分かれた骨片毎に行う．
(3) それぞれの輪郭画像に対して 2.1 で作成した形状モデルを用いて2D/3Dレジストレーションを行い，各骨片の位置姿勢推定を行う．この際，Levenberg-Marquardt 法を用いて最適化し，各骨片の位置姿勢を推定する．
(4) 位置姿勢を固定した状態で，Brent 法[4]を用いて形状モデルのスケールを変化させ，2D/3Dレジストレーションの残差が最も小さくなる値に更新する．
(5) 位置姿勢およびスケールを固定した状態で，形状モデルを(1)式を使用して変形させ，最適な形状に更新する．
(6) (3)～(5)を計算が収束するまで繰返し，X線撮影した骨の形状及び位置姿勢を推定する．

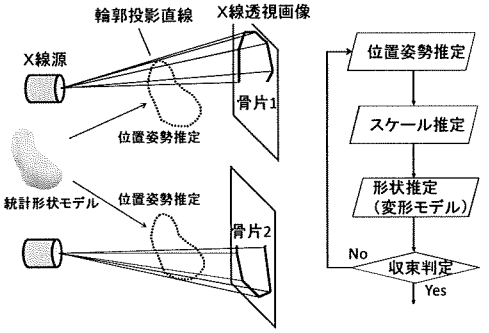

Fig. 1 Schematic diagram of proposed method

3. 実験

提案手法の精度を検証するために，骨折時の舟状骨を用いた骨形状と位置姿勢の推定を行った．比較のために，従来手法による骨形状と位置姿勢の推定を行った．その際，骨折時の舟状骨，骨折時の舟状骨の一部骨片を用いて計算を行った．正常な舟状骨を用い提案手法による計算結果をシステムの限界精度とした．実験には20～30代の男性22名，女性15名(計37名)の手根部を撮影したCT画像を用い，舟状骨（左手）の表面形状モデルを抽出した．このモデルを手法 2.1 に適応し，統計形状モデルを作成した． CT画像を撮影した被験者の舟状骨は正常骨であったため，仮想的に，骨折時を想定した骨折状態の骨の輪郭画像を作成した．その際の画像条件は骨片数 2，画素数 512×512，輪郭点数 150～200 とし，撮影条件は撮影方向 2 方向，2 つの撮影方向の相対角度は 90° とした．得られた統計モデルと輪郭画像を用いて提案手法 2.2 の検証を行った．この時，位置姿勢の初期値を正解値に対して 5mm，5° の標準偏差を与え，試行回数を被験者毎に 50 回とした．形状推定精度の評価には Leave-one-out cross validation 法(Fig. 2)を用いた．この手法は，全サンプルから，一つのサンプルを除き，残りのサンプルでモデルを作成したときに，あらかじめ除いていたサンプルを正確に予測することができるかを検定する方法である．形状推定評価は残差と体積誤差，位置姿勢推定評価は位置誤差と角度誤差を評価項目とした．

Fig. 2 Leave-one-out cross validation method

4. 結果・考察

形状誤差と位置姿勢誤差の結果を，それぞれTable1 と Table 2 に示す．推定位置における骨と正解位置における骨との体積誤差が 40%以上の時，計算が発散したとして除外した．

Table 1 Error of shape estimation

	体積誤差 [%]	平均残差 [mm]	最大残差 [mm]	発散データ数
骨折時に提案手法を適用	12.57	0.35	1.50	1
骨折時の骨片1に従来手法を適用	13.93	0.42	1.72	6
骨折時の骨片2に従来手法を適用	15.90	0.54	2.19	20
骨折時に従来手法を適用	36.54	1.78	5.59	0
正常時に提案手法を適用	10.19	0.28	1.36	0

Table 2 Error of pose estimation

	角度誤差 [deg]			位置誤差 [mm]			発散データ数
	x	y	z	x	y	z	
骨折時に提案手法を適用(骨片1)	1.62	1.78	4.28	0.18	0.31	0.21	23
骨折時に提案手法を適用(骨片2)	4.42	4.31	3.35	0.37	0.43	0.40	91
骨折時の骨片1に従来手法を適用	2.27	1.97	4.36	0.16	0.33	0.22	19
骨折時の骨片2に従来手法を適用	4.83	3.96	3.22	0.29	0.46	0.48	102
骨折時に従来手法を適用	2.47	0.42	1.02	0.14	0.08	0.06	0
正常骨に提案手法を適用	1.41	0.36	0.41	0.06	0.02	0.04	0

提案手法は従来手法に比べ体積誤差，残差共に小さくなり，また収束率が向上した．しかし,位置姿勢誤差では，提案手法と従来手法に大きな差はなかった．提案手法では形状推定時の拘束条件が増えるため形状推定精度が向上するが，位置姿勢推定時は従来手法と拘束条件が同じであるため，妥当な結果であると考えられる．以上から，提案手法を用いることで形状推定精度を向上することができたと考える．

5. 今後の展望

今後は，使用する輪郭の情報量と誤差の関係について未確認であるため，輪郭に応じた誤差解析を行う．また，骨形状と誤差の関係を解析することで，誤差の原因を特定し，精度向上を目指す．

文献

1) 高村俊介ほか，“舟状骨を対象とした2次元X線画像からの3次元骨形状推定法，”第25回日本ロボット学会学術講演会予稿集，2007
2) T.F.Cootes, C.J.Taylot, D.H.Cooper and J.Graham, "Active Shape Models-Their Training and Application," Computer Vision and Image Understanding, vol. 61, pp. 38-59, 1995.
3) Paul J.Besl and Neil D.McKay, "A Method for Rgistration of 3-D Shapes" IEEE Transaction on Pattern Analisys and Machine Intelligence, vol. 14, pp. 239-256, 1992.
4) Brent, Richard P. “Algorithms for minimization without Derivatives (Englewood Cliffs, N.J.: Prentice-Hall), chapter 5, 1973

人体筋骨格モデルに基づく知的医療システムに関する研究

道家 健仁*, 中島 義和**, 小野木 真哉***, 杉田 直彦****, 光石 衛****, 別所 雅彦*****, 大橋 暁*****, 飛田 健治*****, 大西 五三男*****, 佐久間 一郎****, 土肥 健純****, 前田 ゆき******, 小山 毅******, 菅野 伸彦*******, 米延 策雄******, 松本 洋一郎****, 中村 耕三*****

*東京大学工学系研究科, 東京都文京区弥生 2-11-6
**東京大学工学系研究科, 東京大学 IML, 東京都文京区弥生 2-11-6
***東京大学 IML, 東京都文京区弥生 2-11-6
****東京大学工学系研究科, 東京都文京区本郷 7-3-1
*****東京大学医学系研究科, 東京都文京区本郷 7-3-1
******大阪南医療センター, 大阪府河内長野市木戸東町 2 番 1 号
*******大阪大学医学部, 大阪府吹田市山田丘 2-2

do@iml.u-tokyo.ac.jp

要旨

現状の大腿骨骨折整復手術は骨折部の状態を把握するために頻繁に術中 X 線撮影を行っており, 医師を始めとした医療スタッフおよび患者の X 線被曝量の低減が課題となっている. 本研究では, 骨折整復支援ロボットによる, より安全で精確な患者個々に適した整復動作手法の確立を目指す. 下肢の筋肉や靭帯をレオロジー物体とし, パラメータを持ったフォークトモデルを用いて下肢をモデル化した. 力と位置の測定値からパラメータの最適化を行い, 患者個々のパラメータ推定の可能性を検討した. 人体の筋肉・靭帯を模擬したゴムを人工骨に付着させた骨モデルを作製し, 牽引実験を行った. 計測は, ロボットの力センサによる力・トルク計測, 3 次元位置計測装置による大腿骨と足先端の位置に関して行った. その結果, 推定値と実測値の誤差は力 7.8 N, トルク 0.078 Nm となり, 相関値は力が 0.97, トルクが 0.99 と非常に有意な相関を得た. 以上より提案手法による大腿骨位置姿勢推定の可能性が示された.

1. はじめに

近年, 患者側の立場に立った「優しい医療」が求められるようになってきている. その結果として患者の肉体的・精神的負担の軽減を目的とする低侵襲手術への志向が強くなり, 医療経済の面からみても, 効果的な医療が求められている. この低侵襲手術は, 大腿骨骨折整復手術にも普及してきている. 高齢化の影響もあり, 大腿骨骨折整復手術の需要が年々高まっている. しかし, 現状の大腿骨骨折整復手術には 3 つの課題がある. 1 つ目は術中のレントゲン撮影により医師・患者ともに被曝してしまうこと, 2 つ目は術者の体力的負担が大きいこと, 3 つ目は 2 次元の CT 画像からでは整復計画が困難であることである. 特に, 医師ら医療スタッフは, 手術等で X 線被曝の機会が多く, その被曝量低減は重要な課題である. 現在, 骨折整復支援システム[1]の開発が行われており, この整復課題解決のために手術の自動化を目指している.

骨折整復支援システムで使用される骨折整復ロボットは, 患者の足の先端を把持し, 並進・回転をすることで牽引や回旋を任意に行うことが出来る. ロボットの足把持部には力センサが搭載されており, 足先端にかかる力・トルクが計測可能である. しかし, ロボットによる整復動作の際, 外力を加えるロボットと大腿骨骨片の間には足首関節や膝関節があるためロボットと大腿骨の移動量に差異が生まれ, 足把持部に加えた運動が必ずしもそのまま大腿骨骨片の運動にはならない. そのため, 大腿骨を目標とする位置へ移動させるためのロボットの制御法の確立は手術自動化への課題である.

本研究は, 大腿骨骨折整復における大腿骨位置姿勢に対する精確なロボット制御のために, 人体の生体特性[2][3]を考慮したロボットの制御法の確立を目指す.

2. 方法

2.1 大腿骨骨折整復システム

大腿骨骨折整復手術支援システムの構成は大きく分けて，手術ナビゲーションシステムと骨折整復ロボットの２つより構成される．手術ナビゲーションシステムは患者やシステム全体の状態を常に監視し，手術計画と手術シミュレーション，及び骨折整復ロボットへの動作指示を行う．骨折整復ロボットは，手術ナビゲーションシステムの計画・指示に従って実際の整復動作を行う．骨折整復ロボットを図１に示す．骨折整復ロボットは患者の足をブーツで把持し，患脚に対して実際の整復動作を行う．並進３軸，回転３軸の計６軸の駆動軸を有し，回転３軸は１点で交わるように設計されている．また，患者の足に加わる力を計測するために，ロボットは３軸の並進方向の力と３軸のトルクを計測できる力センサを備える．

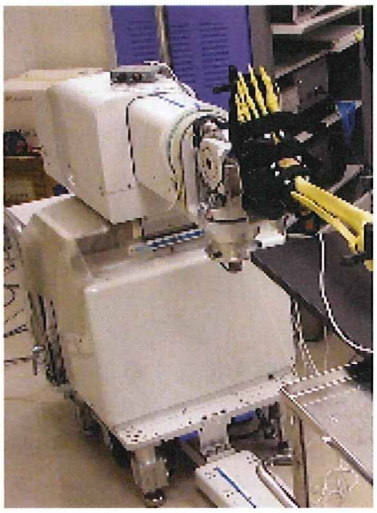

図１　骨折整復ロボット

2.2 筋骨格モデルと生体パラメータの推定

本手法に利用できる情報は，大腿骨に取り付けたマーカによる大腿骨の位置姿勢と，ロボットによる足先の把持部の位置姿勢，ロボットが備える力センサの計測値である．解剖学の知見より，筋肉・靭帯をフォークトモデルで近似しモデルを構築した．筋肉は下肢の主動筋であり，大腿骨骨折整復に影響のある，大腿直筋・ハムストリング・大殿筋を選定し，靭帯は膝関節の靭帯である前十字靭帯・後十字靭帯・内側側副靭帯・外側側副靭帯を選定した．モデルの入力値には各筋肉・人体の長さが必要となる．各付着位置に関して，今回はファントムの実測値を用いたが，実際には標準統計形状モデルを適応させることで各個人に適切な付着位置を得る．回転角度，回転中心軸は計測したマーカの位置姿勢成分から算出する．

まず，各付着位置から靭帯・筋肉の単位方向ベクトルを算出する．

$$\overrightarrow{PQ_i} = \xi_i \vec{e}_x + \eta_i \vec{e}_y + \zeta_i \vec{e}_z \tag{3-1}$$

ここで，脛骨側の付着位置を P_i，大腿骨側の付着位置を Q_i とする．次に，靭帯・筋肉にかかる張力を求める．解剖学の知見より，靭帯・筋肉をバネ・ダンパで近似し，バネとダンパを平行に接続させたモデルを構築する．張力を $F_i(t)$，長さを $L_i(t)$，初期長を $L_i(0)$，バネ定数を k_i，ダンパ定数を c_i，時間を t とする．この時，張力 $F_i(t)$ は

$$F_i(t) = k_i(L_i(t) - L_i(0)) + c_i \frac{\partial L}{\partial t} \tag{3-2}$$

と表すことができる．これを牽引力とトルクに分解する．式(3-1)，(3-2)より牽引力 $F(t)$ は，

$$F(t) = \sum \eta_i \left(k_i(L_i(t) - L_i(0)) + c_i \frac{\partial L}{\partial t} \right) \tag{3-3}$$

となる．同様にトルク $T(t)$ は，

$$T(t)=\sum\left(\xi_i Pz_i-\zeta_i Px_i\right)\left(k_i(L_i(t)-L_i(0))+c_i\frac{\partial L}{\partial t}\right) \tag{3-4}$$

となる．

以上より，筋肉・靭帯の付着位置から長さを求め，足部にかかる力・トルクを算出することが出来る．靭帯・筋肉１つに対するパラメータを i 個，計測データを n 個とすると，１データから $2n$ 個の式が出力される．理論的には，データ数が n ，筋肉・靭帯の生体組織数が i のとき，n が $1.5i$ 以上で方程式を解くことが出来る．実際には取得データ全てを用いた最小二乗法を用いた解の最適化を行い，パラメータの値を決定する．

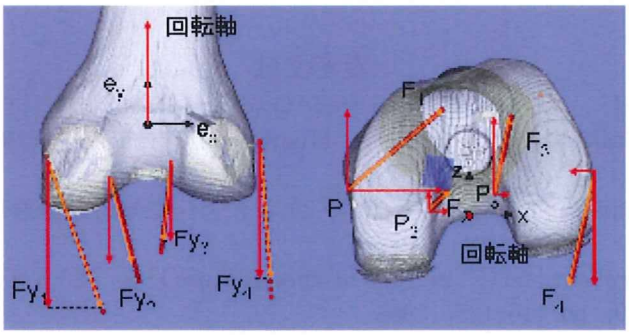

図３　力の分解

2.3　実験

実際に整復動作を行ったデータに対して提案手法が有用であるか検証を行った．実験にはプラスティック骨（SAWBONE，Pacific Research Laboratories，Inc.，USA）に筋肉・靭帯を模したゴムを貼り付けたファントムを使用した．計測はロボットの力センサによる力・トルク計測，３次元位置計測装置（OPTOTRAK™，Northern Digital Inc.，Canada）による大腿骨と足先端の位置計測を行い，牽引，回旋，牽引回旋の３種類の動作を行った．

3．結果

実験の結果を以下に述べる．回旋の結果を図５，図６に示す．力，トルクともに実測値に近い傾向を示した．推定値と実測値の誤差は力 7.8 N，トルク 0.078 Nm となった．牽引動作，牽引回旋動作では，力，トルクともに誤差が大きくなったが，推定値と実測値は同じ傾向を示し，相関値は力が 0.97，トルクが 0.99 と非常に有意な相関を得た．

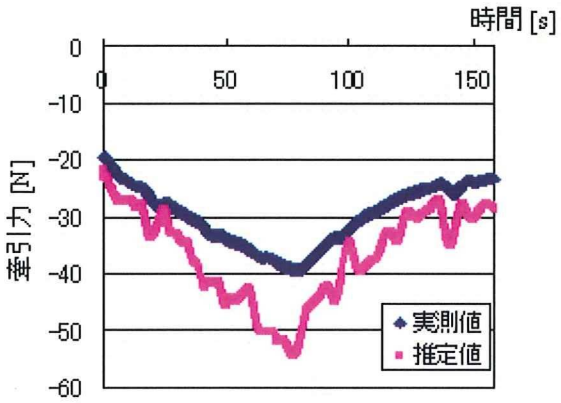

図５　回旋時の力の比較

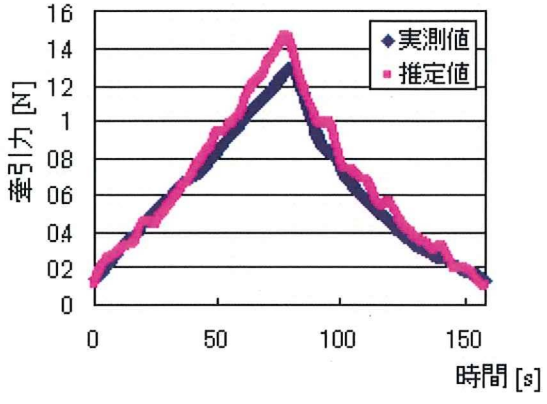

図６　回旋時のトルクの比較